npj | Quantum Materials

www.nature.com/npjquantmats

ARTICLE OPEN

Designing new ferroelectrics with a general strategy

Ke Xu[1,2,4], Xue-Zeng Lu[3] and Hongjun Xiang[1,4]

The presence of a switchable spontaneous electric polarization makes ferroelectrics ideal candidates for the use in many applications such as memory and sensors devices. Since known ferroelectrics are rather limited, finding new ferroelectric materials has become a flourishing field. One promising route is to design the improper ferroelectrics. However, previous approach based on the Landau theory is not easily adopted for systems that are unrelated to the *Pbnm* perovskite structure. To this end, we develop a general design rule that is applicable to any system. By combining this rule with the density functional theory calculations, we identify previously unrecognized classes of ferroelectric materials. It is shown that the $R\bar{3}c$ perovskite structure can become ferroelectric by substituting half of the B-site cations. Compound $ZnSrO_2$ with a non-perovskite layered structure can also be ferroelectric through the anion substitution. Moreover, our approach can be used to design new multiferroics as illustrated in the case of fluorine substituted $LaMnO_3$.

npj Quantum Materials (2017)2:1 ; doi:10.1038/s41535-016-0001-8

INTRODUCTION

Recently ferroelectrics (FEs) have attracted much attention due to their wide range of applications, especially in the electronic devices such as nonvolatile memory,[1,2] tunable capacitors,[3] solar cell,[4] and tunnel junction.[5] For traditional proper FEs, such as $BaTiO_3$, the transition metal ion Ti^{4+} with d^0 configuration can hybridize with the oxygen 2p states leading to the FE phase transition due to the pseudo Jahn-Teller effect.[6–10] However, FEs are very few in nature.[11] To find more high-performance FEs, improper (including hybrid improper) FEs become an intense research field.[12] The typical example of the conventional improper FEs is hexagonal manganite $YMnO_3$,[13] where the FE buckling (P mode) of the Y-O planes is induced by the non-polar MnO_5 polyhedra tilt (Q mode).[13,14] The free energy expansion in this system contains the coupling term (PQ^3) between the Q and P, indicating that the non-polar distortion Q must be reversed.[15] The hybrid improper ferroelectricity (HIF) was recently discovered in the artificial superlattice $PbTiO_3/SrTiO_3$,[16] where the ferroelectricity is induced by a trilinear coupling (PQ_1Q_2) between the FE mode (P) and two oxygen octahedral rotational modes (Q_1 and Q_2, respectively). The HIF was also found in the double-layered Ruddlesden-Popper (RP) perovskite $A_3B_2O_7$ (A=Ca, Sr; *B*=Mn,Ti),[17–19] the 1:1 A-cation ordering perovskite-type superlattice,[20–23] A-cation ordering RP $NaRTiO_4$ (*R* = Y, La, Nd, Sm-Ho),[24] the 2:2 B-cation ordered superlattice,[25] and metal-organic perovskite material.[26]

In the above-mentioned theoretically designed FEs, one usually starts from a high-symmetry structure (e.g., cubic perovskite structure), then the effect of atomic substitution and soft phonon modulations are examined to see whether the ferroelectricity can be induced or not. Finally, the trilinear coupling mechanism is discussed to understand the origin of improper ferroelectricity. This procedure is indeed informative. However, it is tedious and its applicability to other type of compounds is limited since even the high-symmetry structure may be unknown. Therefore, two key questions remain to be addressed: Is it possible to propose a general method to design improper FEs? Can improper ferroelectricity be obtained in systems with totally different structures from perovskite? The answers to these questions may widen the opportunities of finding the improper FE materials. In this work, we propose a general approach to design the FE materials. Our approach can not only reproduce the previous results (e.g., the 1:1 A-cation [001] ordered FE perovskite superlattices), but also predict new FEs. Our results show that the B-cation ordered$[11\bar{1}]$-superlattice$La_2(Co,Al)O_6$ with a $R\bar{3}c$ parent structure displays a spontaneous polarization. And compound $ZnSrO_2$ with a non-perovskite layered structure can also be FE by proper anion substitution. Moreover, compound $LaMnO_3$with the fluorine substitution can become multiferroic of a sizable polarization with its direction perpendicular to the direction of magnetization. Hence, our study may pave a new route to find the FE materials.

RESULTS

General design guidelines

Firstly, the parent structure should have the true inversion centers (TICs) and pseudo inversion centers (PICs) simultaneously and also have a sizable band gap. The TIC is defined as a position on which there is inversion symmetry *I* of the structure. The PIC is a position which can become a TIC after small displacements of the atoms. With a given centrosymmetric structure (i.e., parent structure), we first find all the TICs and PICs. Then we find out all the possible atom substitutions within a given supercell of the parent structure, which lift all the TICs but still keep at least one PIC. These substituted structures can be candidates for FEs. After the slight displacements of the ions in a substituted structure where the PIC becomes a TIC, the corresponding paraelectric (PE) structures can

[1]Key Laboratory of Computational Physical Sciences (Ministry of Education), State Key Laboratory of Surface Physics, and Department of Physics, Fudan University, Shanghai 200433, People's Republic of China; [2]Hubei Key Laboratory of Low Dimensional Optoelectronic Materials and Devices, Hubei University of Arts and Science, Xiangyang 441053, People's Republic of China; [3]Department of Materials Science and Engineering, Northwestern University, Evanston, IL 60208, USA and [4]Collaborative Innovation Center of Advanced Microstructures, Nanjing 210093, People's Republic of China
Correspondence: Hongjun Xiang (hxiang@fudan.edu.cn)

Received: 14 July 2016 Revised: 28 October 2016 Accepted: 14 November 2016

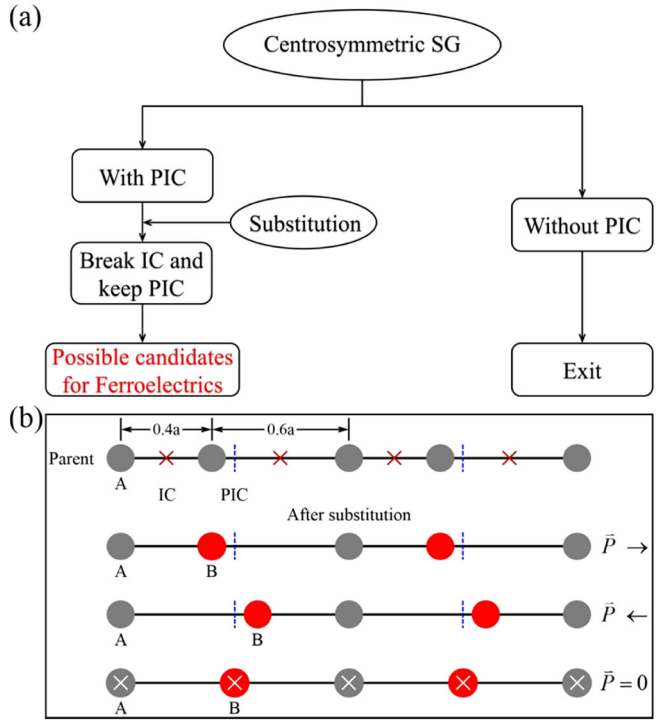

Fig. 1 Flow chart and diagrammatic sketch of our method. **a** The flow chart of our method for designing new ferroelectrics. **b** A simple one-dimensional model system to illustrate the idea of our method. The position 0.5a is the pseudo inversion centers (PICs) and denoted by the vertical dashed line. The true inversion centers (TICs) are denoted by "×". "SG" is an abbreviation for "space group"

be obtained. Figure 1a shows a chart for the general strategy of designing new FEs. Our method is illustrated clearly with a simple one-dimensional toy model (see Fig. 1b). Assuming that there is a one-dimensional chain with two atoms of the same type (represented by A) in a unit cell, the two atoms locate at positions 0.0 and 0.4, respectively. Then, one can find two TICs denoted by the crosses within a unit cell before any substitution. If replacing an A atom by a B atom in the unit cell, all the TICs disappear, resulting in a possible polar structure with polarization P along the left or right directions. However, there is a PIC at position 0.5 even after the substitution. When moving the B atom to the center of the unit cell, the PIC will become a TIC. From the above discussion, the key point in our method is lifting all the TICs by proper atomic substitution and maintaining at least one PIC in the system. To ensure the successful design of FEs, we need two additional conditions: (I) The FE phase should be locally stable; (II) Both the FE and PE phases should have large band gaps. Since the superlattice-type structures may be synthesized by means of the molecular beam epitaxy methods, we hereafter mainly focus on the superlattice-type structures.

Improper FEs based on the *Pbnm* ABO_3 perovskite structure

Let us first concentrate on the design of FEs based on ABO_3 perovskites. The *Pbnm* structure with 20 atoms in the unit cell can be obtained if the cubic $Pm\bar{3}m$ structure undergoes an out-phase rotation and in-phase rotation of oxygen octahedral ($a^-a^-c^0$ and $a^0a^0c^+$in Glazer notation, respectively).[11] By using our method, we find that there are 8 TICs (all B-sites are TICs) and 24 PICs in one unit cell of the *Pbnm* structure (see Fig. SI in the Supplementary Information (S1) for details). Within the 20-atom cell, 14 possible substitution-induced FEs in total are found, with 2 types of A-site substitutions and 12 types of anion substitutions (see Fig. S2 in the SI). One of the A-site substituted $(A/A')B_2O_6$, is the [001] FE superlattice discovered in previous studies.[20–23] The A and A′-site ordering breaks all the TICs but maintains the 16 PICs. The appearance of net electric polarization is due to the fact that the A-site displacement and the A′-site displacement are not completely cancelled. We find that it is impossible to obtain improper FEs through B-site substitutions in a 20-atom cell, in agreement with previous result.[22] Nevertheless, considering a twofold supercell along the **z** direction, we can obtain FEs by any B-site substitution. For example, our result indicates that the B/B′ cation ordered 2/2 supercell adopts the FE $Pmn2_1$ symmetry (see Fig. S3 in the SI for the possible substitutions in the 2/2 B/B′′ cation ordered superlattices). All these results demonstrate that our method can not only reproduce the earlier reported results,[20–23] but also predict previously unknown FE materials. In particular, we point out for the first time that the anion substitution may lead to improper ferroelectricity, to be discussed later in details.

Improper FEs based on the $R\bar{3}c$ ABO_3 perovskite structure

Another family of perovskite oxides favor the 10-atom $R\bar{3}c$ structure as the lowest energy structure,[27] which has a rhombohedral $a^-a^-a^-$ tilt pattern around the [111] direction with respect to the $Pm\bar{3}m$ structure. There are eight TICs and eight PICs in one unit cell (the B-sites are TICs). Within the 10-atom cell, we find that there are two possible ways of the anion substitutions to induce improper FE (see Fig. S4 a, b in the SI). If considering a twofold 20-atom supercell, one has three types of FEs which result from the A-site, B-site and C-site substitutions, respectively (see Fig. S5 b, c and in the SI for the A-site, B-site, and C-site substitutions). Note that the A-site order in the 1:1 superlattice exhibits the non-FE structure with the *R*32 symmetry.[28]

In the following, $LaCoO_3$ and $LaAlO_3$ are selected as the parent structures to demonstrate the B-site substitution induced ferroelectricity in the $R\bar{3}c$ ABO_3 perovskites. It was experimentally known that $LaCoO_3$ and $LaAlO_3$ take the $R\bar{3}c$ structure as the ground state, which is also confirmed by our test calculations. The mismatch in the lattice constants between these two compounds is only about 0.13%. $LaCoO_3$ with the$R\bar{3}c$ symmetry adopts a low-spin nonmagnetic ground state[29–31] (t_{2g}^6, $S=0$) for Co^{3+}. For all the perovskites with the$R\bar{3}c$ symmetry, we find that the $[11\bar{1}]$ B-site order in the 1:1 20-atom superlattice results in a polar structure with the *C*2 symmetry. The corresponding PE structure takes the $R\bar{3}m$ symmetry. Both the FE and PE structures have large band gaps about 2.0 eV, and the energy barrier between the FE and PE structures is ~0.3 eV for a 20-atom cell. This spontaneous electric polarization is calculated to be 0.5 μC/cm^2, aligning along the $[1\bar{1}0]$ direction. The ferroelectricity is caused by the fact that the B-site inversion symmetry is broken by the B-site substitution. For clarity, we show the local structures of $LaAlO_3$ and La_2CoAlO_6 to understand the direction of polarization. A 10-atom $La_3Al_4O_3$ cluster in the $R\bar{3}c$ $LaAlO_3$ forms a tetrahedral structure. This cluster has one out-of-plane threefold-rotational axis on the central Al atom and three in-plane twofold-rotational axes along the La–La bond directions (see Fig. 2a). In La_2CoAlO_6 with a $[11\bar{1}]$ B-site order, only one twofold rotation axis is kept due to the Co-atom substitution. This twofold rotation axis is exactly along the direction of polarization (see Fig. 2b). Interestingly, we find that the direction of polarization $\mathbf{P}[1\bar{1}0]$ is parallel to the cross product of the B-site ordering vector $\mathbf{D}[11\bar{1}]$ and the octahedral rotational vector **Ω** [111] (see Fig. 2c), i.e.,$\mathbf{P}\|\mathbf{D}\times\mathbf{\Omega}$. This relation also holds for the other FE domains (There are six different domains since the octahedron rotation **Ω** may have six possible rotation directions: [111], [−1−1−1], [1−1−1], [−1,1,1], [1−11], [−11−1], and [−1−1−1]). The phonon dispersion also shows that the superlattice is stable (see Fig. S8 in the SI). In addition, our genetic algorithm (GA)[32] structure search confirms that the FE *C*2 structure is indeed the lowest energy structure.

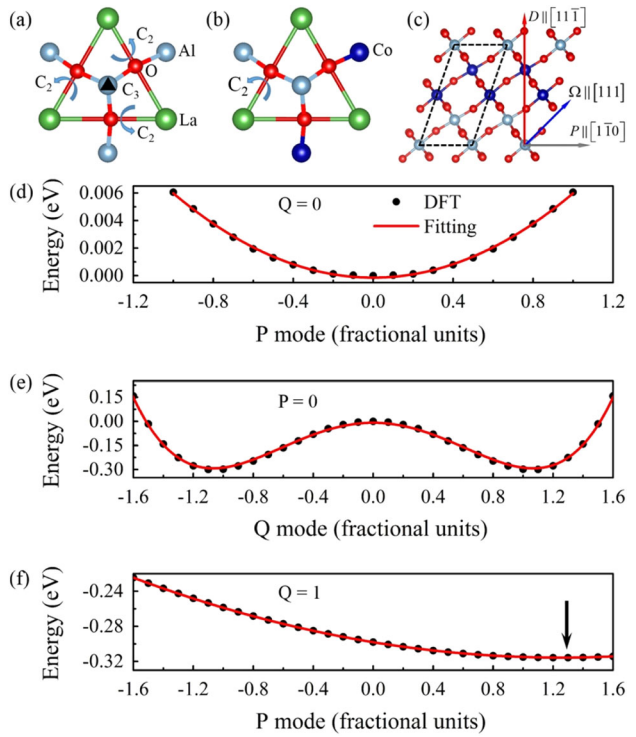

Fig. 2 B-site substitution induced ferroelectricity in $R\bar{3}c$ perovskite system. **a** Shows the structure of the $La_3Al_4O_3$ cluster in $R\bar{3}c$ $LaAlO_3$. The corresponding structure of the $La_3Co_2Al_2O_3$ cluster in $C2$ $La_2(Co,Al)O_6$ is displayed in **b**, **c** The structure of the FE $C2$ $La_2(Co,Al)O_6$. The A-site La atoms are not shown for clarity. The direction of polarization P is perpendicular to both the superlattice direction D and the rotation direction Ω of the oxygen octahedron. **d**, **e** Show the total energies of $La_2(Co,Al)O_6$ as a function of the magnitudes of the P mode and the Q mode, respectively. **f** Total energies of $La_2(Co,Al)O_6$ as a function of the magnitude of the P mode with a fixed Q mode ($Q = 1$). For simplicity, we adopt the fractional unit for the P and Q modes, i.e., we rescale the P and Q to the dimensionless quantities: $P = 1$ and $Q = 1$ mean that the total displacements of P and Q modes are equal to 0.0496 and 0.8218 Å respect to the 20-atom $R\bar{3}2/m$ $La_2(Co,Al)O_6$ PE structure. The *black arrow* indicates the lowest energy point

For proper FEs, the FE mode is the primary order parameter and there is a double well potential in the plot of energy versus polar displacement. But for the improper FEs, the FE mode is no longer the primary order parameter, i.e., the polarization is induced by one or two rotational modes.[13–25] To verify whether the $[11\bar{1}]$-superlattice $LaCoO_3/LaAlO_3$ is an improper FE or not, the stability of the FE mode will be examined. We adopt the ISOTROPY software[33] to obtain the symmetry-adapted phonon modes in the low-symmetry FE structure. To find out the appropriate FE mode and eliminate the effect of the symmetry breaking solely due to atomic substitution, we first replace the Co atoms in $La_2(Co,Al)O_6$ back to Al atoms before allowing the mode decomposition with respect to the cubic $Pm\bar{3}m$ $LaAlO_3$. We find two dominant modes, namely, FE mode and rotation mode. Hereafter, we will refer to these two modes as 'polar' and 'rotation' modes, respectively. Note that the PE structure is not $R\bar{3}2/m$ here. After this mode decomposition, we replace the Al atoms back to Co, in order to obtain the PE reference structure $La_2(Co,Al)O_6$ with the $R\bar{3}2/m$ symmetry. The corresponding FE structure has the $C2$ symmetry. Second, we find that the earlier identified 'polar' and 'rotation' modes are both composed by the non-degenerate Γ_1^- and double degenerateΓ_3^- normal modes of the $La_2(Co,Al)O_6R\bar{3}2/m$ PE structure. The Γ_3^- mode is the two-dimensional irreducible representation in active D_{3d} point group and can induce the in-plane polarization but the Γ_1^- mode is non-polar. Here, we redefine the Γ_3^-components of the 'polar' and 'rotation' modes as P and Q modes, respectively. Our group theoretical analysis shows that the Landau free energy can be expanded in terms of P(P_x,P_y) and Q (Q_x,Q_y) around the reference $R\bar{3}2/m$ structure:

$$F[(P_x,P_y);(Q_x,Q_y)] = a(P_x^2+P_y^2)+b(Q_x^2+Q_y^2) + c(Q_x^2+Q_y^2)^2 + d(P_xQ_x+P_yQ_y) \quad (1)$$

The last term of the free energy is the linear coupling between the P and Q modes, which is allowed since they belong to the same representation of the $R\bar{3}2/m$ space group. For simplicity, we rescale the P and Q to the dimensionless quantities: $P = 1$ and $Q = 1$ mean that the total displacements of the P and Q modes are equal to 0.0496 and 0.8218 Å with respect to the 20-atom $R\bar{3}2/m$ $La_2(Co,Al)O_6$ PE structure, respectively. When applying the FE P mode to the PE structure, we find that the total energy increases with the mode magnitude, and thus the FE P mode is not a soft mode. For the Q mode, it has a double well potential in the plot of energy versus Q mode displacement (see Fig. 2d). These characteristics indicate that the layered $(LaAlO_3)_1/(LaCoO_3)_1$ superlattice is an improper FE. The four parameters a, b, c and d of the Landau free energy can be obtained by a fitting of the density functional theory (DFT) results. We can see that the DFT is described rather well by the simple form of the Landau free energy (see Fig. 2d–f). The obtained parameters are $a = 0.00612$ eV, $b = -0.49735$ eV, $c = 0.21836$ eV, and $d = -0.02829$ eV, respectively. Since d is important, it is expected that the linear coupling between the P and Q modes will induce a finite FE P mode although the P mode itself is not unstable ($a > 0$).

New FEs based on the non-perovskite structures

Previous works on designing improper FEs mainly focused on the perovskite-related structures. We note that if a crystal structure has the TIC, PIC, and band gap simultaneously, it is a possible parent candidate for designing new FEs through atom substitution. Here, we find that the non-perovskite structure $ZnSrO_2$ with the *Pnma* symmetry is suitable for such FEs design. We note that the experimentally synthesized $ZnSrO_2$ compound is a metastable structure since the formation energy of $ZnSrO_2$ is positive with respect to the rock salt SrO and wurtzite ZnO. The parent structure with eight TICs and eight PICs has a large direct band gap ~2.2 eV at the Perdew-Burke-Ernzerhof level. The unit cell can be regarded as a layered structure along the z direction that contains two formula units of $Zn_2Sr_2O_4$, in which there exist three twofold screw axes 2_1 as shown in Fig. 3a. By replacing the outer O atoms of the upper $ZnSrO_2$ layer with S atoms, we obtain a FE $Pmc2_1$ structure of $Zn_4Sr_4O_6S_2$. The corresponding PE structure has the *Pmma* symmetry. The energy barrier between the FE and PE states is ~0.4 eV. The replacement of the oxygen atoms with the two sulfur atoms in a unit cell will break the screw axes along the **a** and **c** directions and induce a large spontaneous polarization (~20.0 μC/cm^2) along the **b** direction (see Fig. 3b). The large polarization is due to the large atomic displacements induced by the sulfur replacement. Figure. 3b shows the atomic direction and magnitude of the displacement (see red arrows) after the full relaxation. The S atom is nearly at the original O position. Because the bond length of Zn-S is larger than that of Zn-O, Zn_1 and Zn_2 ions move along the **–c** or **c** directions, respectively. This subsequently leads to a large displacement of the O_2 atom along the direction (i.e., approximately [011] direction) perpendicular to the Zn_1-Zn_2bond direction. Overall, these ion displacements induce a large polarization along the **–b** axis in the relaxed structure of $Zn_4Sr_4O_6S_2$. Moreover, the new FEs $Zn_4Sr_4O_6S_2$ is an environmentally friendly non-toxic material unlike $PbTiO_3$.

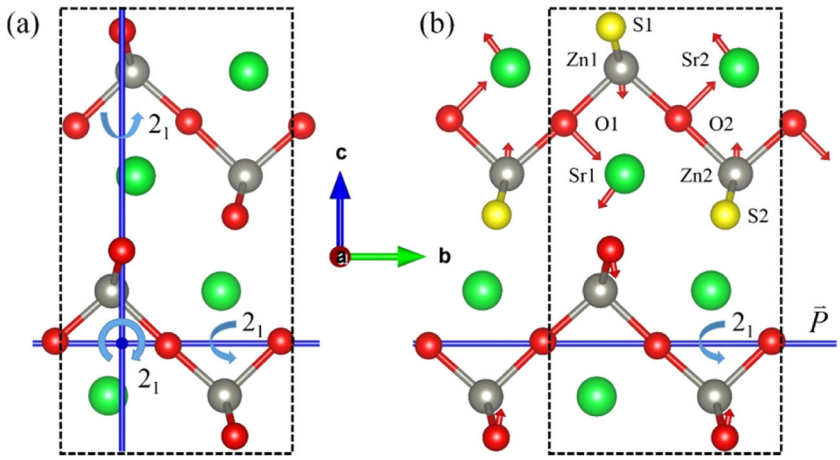

Fig. 3 Anion substitution induced ferroelectricity in $ZnSrO_2$ with a non-perovskite structure. **a** The original structure of $ZnSrO_2$. The three screw axes are shown. **b** The FE structure of $Zn_4Sr_4O_6S_2$ obtained by replacing one fourth of the oxygen atoms with sulfur atoms. After the anion substitution, only the screw axis along the b axis is kept, resulting in a polarization along the b axis. The atomic displacements after relaxation are denoted by *red arrows*

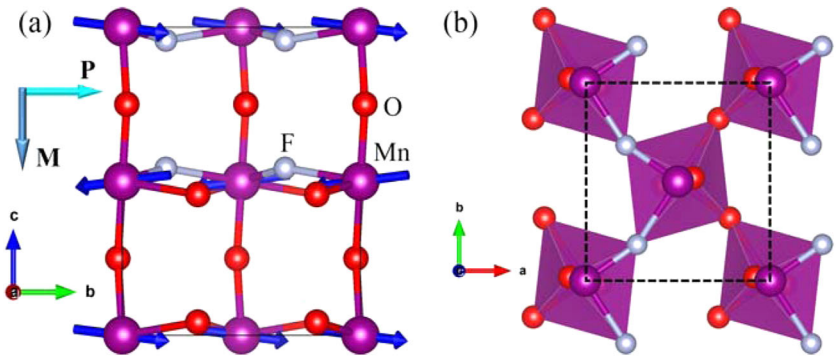

Fig. 4 Design multiferroics based on perovskite structure. Multiferroic $SrMnO_2F$ obtained by replacing one third of O ions by F ions in *Pbnm* $LaMnO_3$ (La ions are also replace by Sr ions to maintain the number of valence electrons). **a** The geometry and magnetic structure of $SrMnO_2F$. The Mn^{3+} magnetic moments are denoted by *blue arrows*. Note that the canting of the magnetic moments along the c axis is exaggerated to guide the eye. The directions of the total electric polarization (P) and total canted moment (M) are depicted. **b** A polyhedral representation of the $SrMnO_2F$ structure viewed along the orthorhombic c direction, which clearly shows the superlattice ordering of F and O ions along the orthorhombic a direction. The A-site cations are not shown for clarity

Multiferroics based on the anion-substituted perovskite compound

Our method is also suitable for designing new multiferroics. It is well-known that the ground state of $LaMnO_3$ is A-type antiferromagnetic (A-AFM) with *Pbnm* space group.[34] Thus, $LaMnO_3$ is selected as a parent structure for illustration. One can obtain a FE structure by replacing one-third of oxygen atoms with fluorine atoms to form a superlattice along the orthorhombic **a** direction (see Fig. 4a, b). We note that the replacement of oxygen ions in perovskite oxides by other anions such as fluorine ions has been achieved experimentally.[35–37] Since La and Mn ions in the parent $LaMnO_3$ structure are both trivalent, we also replace all the A-site La ions with bivalent Sr ions, whose radius is very similar to that of La^{3+}. The chemical formula of the final substituted structure becomes $SrMnO_2F$. The FE and PE $SrMnO_2F$ phases take the polar $Pmc2_1$ and non-polar *Pbcm* symmetries, respectively. The $SrMnO_2F$ is also an improper FE, see Fig. S10 in the SI for details. The electric polarization of the FE structure is 14.5 μC/cm^2 along the orthorhombic **b** direction. We find that the magnetic ground states for both FE and PE structures of $SrMnO_2F$ are the A-AFM, which are similar to the parent structure of $LaMnO_3$.[34] When considering the spin-orbit coupling effect, $SrMnO_2F$ displays a magnetic anisotropy with the magnetic easy axis along the orthorhombic **b** direction. The Dzyaloshinskii-Moriya interaction[38,39] leads to a canted ferromagnetic magnetic moment of about 0.058 μ_B along the orthorhombic **c** direction. In the parent structure of $LaMnO_3$, the total canted magnetic moment is 0.027 μ_B, which indicates that the anion substitution not only induces the ferroelectricity, but also increases the canted magnetic moment. Since the $SrMnO_2F$ with the $Pmc2_1$ structure has both weak ferromagnetism and ferroelectricity, it is a multiferroic. In addition, we find that the $LaMnO_2F$ with the FE $Pmc2_1$structure has a G-type antiferromagnetic order with a very small magnetic anisotropy since the Mn^{2+} ion is half-filled.

CONCLUSION

In conclusion, we have proposed a general method to design new FEs. We note that whether the designed FE is proper or improper is an open question. With this method, we can not only rediscover the HIF in A-site [001] ordered *Pbnm* perovskite oxides, but also discover new improper FEs. In particular, our results show that the B-site ordered$[11\bar{1}]$ superlattice $(LaCoO_3)_1/(LaAlO_3)_1$can be an improper FE. We also demonstrate for the first time that the

anion substitution can be adopted to generate FEs as exemplified in the case of perovskite systems and $ZnSrO_2$ with a non-perovskite structure. Moreover, through the cation and anion substitution in $LaMnO_3$, we find that $SrMnO_2F$ is a multiferroic, which indicates that our method is also useful for the design of multiferroic materials.

METHODS

Strategy for finding PICs

The inversion center in a three-dimensional crystalline structure must locate at an atomic site or the center of two identical-element atoms. In our strategy for finding the PICs, we first consider all the possible inversion centers. For each possible inversion center, we first check whether it is a TIC or not. If yes, it is a TIC instead of a PIC. If not, we will consider whether it becomes a TIC after we displace the atoms in a given range (e.g., less than 2.0 Å).

The element substitution may remove some of the TICs and PICs. It is also possible that some element substitution strategies will keep some of the TICs and PICs. For each substitution case, we check whether it breaks all the TICs but keeps at least one PIC. If yes, this substitution will lead to a possible realization of ferroelectricity.

Electronic calculations

In this work, the geometry optimization and electron structure calculation are performed by the state-of-the-art DFT[40] using the projector augmented-wave[41] potentials as implemented in the Vienna ab-initio Simulation Package.[42,43] In the DFT plane-wave calculations, the plane wave cutoff energy is set to 500 eV, and the exchange-correlation interactions are described by the Perdew–Burke–Ernzerhof generalized gradient approximation (GGA).[44] In order to take into account for the proper orbital dependence of the on-site Coulomb and exchange interactions, we employ the GGA + U method[45] in treating the Co's and Mn's 3d orbitals and the values of U are set to 7.0 and 3.0 eV, respectively. For the relaxation of structures, the Hellmann-Feynman forces on each atoms are less than 0.001 eV/Å. The total electric polarization is calculated using the Berry phase method.[46,47]

Global optimization

We adopt a global optimization method based on the GA[32] to search for the ground state of layered compound La_2CoAlO_6. In our calculation, the basic lattice structure is fixed and our purpose is to find the distortions that leads to the lowest energy. It means that the basic framework (perovskite-type in current case) is fixed, but the structural distortions (FE displacements, oxygen octahedron rotations, cell deformation etc.) are allowed. In this GA searching method, the DFT calculation is adopted to relax the structure and the low-spin configuration is adopted for Co. The number of atoms in the supercell is fixed to 20. The population size and number of generations are set to 16 and 10, respectively.

ACKNOWLEDGEMENTS

Work at Fudan was supported by NSFC, Research Program of Shanghai Municipality and MOE, the Special Funds for Major State Basic Research (2015CB921700), Qing Nian Ba Jian Program, Program for Professor of Special Appointment (Eastern Scholar), and Fok Ying Tung Education Foundation. K. X. was partially supported by NSFC 11404109. X. L. was supported in part by the National Science Foundation (NSF) through the Pennsylvania State University MRSEC under award number DMR-1420620, which is supervised by Prof. James M. Rondinelli. We thank Panshuo Wang for useful comments on the manuscript.

AUTHOR CONTRIBUTIONS

The study was proposed and planned by H.X. The calculations were carried out by K. X. All authors discussed the results and wrote the manuscript.

COMPETING INTERESTS

The authors declare no conflict of interests.

REFERENCES

1. Liao, L. *et al.* Ferroelectric transistors with nanowire channel: toward nonvolatile memory applications. *ACS Nano* **3**, 700–706 (2009).
2. Garcia, V. & Bibes, M. Electronics: inside story of ferroelectric memories. *Nature* **483**, 279–281 (2012).
3. Jamil, A. & Kalkur, T. S. Tunable ferroelectric capacitor-based voltage-controlled oscillator. *IEEE Transact. Ultrason. Ferr.* **54**, 222–226 (2007).
4. Choi, T. *et al.* Switchable ferroelectric diode and photovoltaic effect in $BiFeO_3$. *Science* **324**, 63–66 (2009).
5. Garcia, V. *et al.* Ferroelectric control of spin polarization. *Science* **327**, 1106–1110 (2010).
6. Burdett, J. K. Use of the Jahn-Teller theorem in inorganic chemistry. *Inorg. Chem.* **20**, 1959–1962 (1981).
7. Kunz, M. & Brown, I. D. Out-of-center distortions around octahedrally coordinated d^0 transition metals. *J. Solid State Chem.* **115**, 395–406 (1995).
8. Bersuker, I. B. Modern aspects of the Jahn–Teller effect theory and applications to molecular problems. *Chem. Rev.* **101**, 1067–1114 (2001).
9. Bersuker, I. B. Pseudo-Jahn-Teller effect-a two-state paradigm in formation, deformation, and transformation of molecular systems and solids. *Chem. Rev.* **113**, 1351–1390 (2013).
10. Rondinelli, J. M., Eidelson, A. S. & Spaldin, N. A. Non-d^0 Mn-driven ferroelectricity in antiferromagnetic $BaMnO_3$. *Phys. Rev. B* **79**, 205119 (2009).
11. Benedek, N. A. & Fennie, C. J. Why are there so few perovskite ferroelectrics? *J. Phys. Chem. C.* **117**, 13339–13349 (2013).
12. Benedek, N. A. *et al.* Understanding ferroelectricity in layered perovskites: new ideas and insights from theory and experiments. *Dalton Trans.* **44**, 10543–10558 (2015).
13. Van Aken, B. B., Palstra, T. T. M., Filippeti, A. & Spaldin, N. A. The origin of ferroelectricity in magnetoelectric $YMnO_3$. *Nat. Mater.* **3**, 164–170 (2004).
14. Fennie, C. J. & Rabe, K. M. Ferroelectric transition in $YMnO_3$ from first principles. *Phys. Rev. B.* **72**, 100103 (2005). (R).
15. Young, J., Stroppa, A., Picozzi, S. & Rondinelli, J. M. Anharmonic lattice interactions in improper ferroelectrics for multiferroic design. *J. Phys.: Condens. Matter* **27**, 283202 (2015).
16. Bousquet, E. *et al.* Improper ferroelectricity in perovskite oxide artificial superlattices. *Nature* **452**, 732–736 (2008).
17. Benedek, N. A. & Fennie, C. J. Hybrid improper ferroelectricity: a mechanism for controllable polarization-magnetization coupling. *Phys. Rev. Lett.* **106**, 107204 (2011).
18. Oh, Y. S. *et al.* Experimental demonstration of hybrid improper ferroelectricity and the presence of abundant charged walls in $(Ca,Sr)_3Ti_2O_7$ crystals. *Nat. Mater.* **14**, 407–413 (2015).
19. Liu, X. Q. *et al.* Hybrid improper ferroelectricity in Ruddlesden-Popper $Ca_3(Ti,Mn)_2O_7$ ceramics. *Appl. Phys. Lett.* **106**, 202903 (2015).
20. Mulde, A. T., Benedek, N. A., Rondinelli, J. M. & Fennie, C. J. Turning ABO_3 antiferroelectrics into ferroelectrics: design rules for practical rotation-driven ferroelectricity in double perovskites and $A_3B_2O_7$ Ruddlesden-Popper compounds. *Adv. Funct. Mater.* **23**, 4810–4820 (2013).
21. Young, J. & Rondinelli, J. M. Atomic scale design of polar perovskite oxides without second-order Jahn –Teller Ions. *Chem. Mater.* **25**, 4545–4550 (2013).
22. Rondinelli, J. M. & Fennie, C. J. Octahedral rotation-induced ferroelectricity in cation ordered perovskites. *Adv. Mater.* **24**, 1961–1968 (2012).
23. Zhao, H. J., Íñiguez, J., Ren, W., Chen, X. M. & Bellaiche, L. Atomistic theory of hybrid improper ferroelectricity in perovskites. *Phys. Rev. B.* **89**, 174101 (2014).
24. Balachandran, P. V., Puggioni, D. & Rondinelli, J. M. Crystal-chemistry guidelines for noncentrosymmetric A_2BO_4 Ruddlesden–Popper oxides. *Inorg. Chem.* **53**, 336–348 (2014).
25. Zhang, H. M., Weng, Y. K., Yao, X. Y. & Dong, S. Charge transfer and hybrid ferroelectricity in $(YFeO_3)_n/(YTiO_3)_n$ magnetic superlattices. *Phys. Rev. B.* **91**, 195145 (2015).
26. Stroppa, A., Barone, P., Jain, P., Perez-Mato, J. M. & Picozzi, S. Hybrid improper ferroelectricity in a multiferroic and magnetoelectric metal-organic framework. *Adv. Mater.* **25**, 2284–2290 (2013).
27. Lufaso, M. W. & Woodward, P. M. Prediction of the crystal structures of perovskites using the software program SPuDS. . *Acta Cryst. B.* **57**, 725–738 (2001).
28. Young, J. & Rondinelli, J. M. Improper ferroelectricity and piezoelectric responses in rhombohedral $(A, A')B_2O_6$ perovskite oxides. *Phys. Rev. B.* **89**, 174110 (2014).
29. Thornton, G., Tofield, B. C. & Hewat, A. W. A neutron diffraction study of $LaCoO_3$ in the temperature range $4.2 < T < 1248$ K. *J. Solid State Chem.* **61**, 301–307 (1986).
30. Louca, D., Samo, J. L., Thompson, J. D., Rodes, H. & Kari, G. H. Correlation of local Jahn-Teller distortions to the magnetic/conductive states of $La_{1-x}Sr_xCoO_3$. *Phys. Rev. B.* **60**, 10378–10382 (1999).
31. Radaelli, P. G. & Cheong, S. W. Structural phenomena associated with the spin-state transition in $LaCoO_3$. *Phys. Rev. B.* **66**, 094408 (2002).

32. Lu, X. Z., Gong, X. G. & Xiang, H. J. Polarization enhancement in perovskite superlattices by oxygen octahedral tilts. *Comput. Mater. Sci.* **91**, 310–314 (2014).
33. Campbell, B. J., Stokes, H. T., Tanner, D. E. & Hatch, D. M. *ISODISPLACE*: a web-based tool for exploring structural distortions. *J. Appl. Crystallogra.* **39**, 607–614 (2006).
34. Moussa, F. *et al.* Spin waves in the antiferromagnet perovskite $LaMnO_3$: A neutron-scattering study. *Phys. Rev. B.* **54**, 15149–15155 (1996).
35. Tsujimoto, Y., Yamaura, K. & Muromachi., E. T. Oxyfluoride chemistry of layered perovskite compounds. *Appl. Sci.* **2**(1), 206–219 (2012).
36. Moon, E. J. *et al.* Fluorination of epitaxial oxides: synthesis of perovskite oxyfluoride thin films. *J. Am. Chem. Soc.* **136**, 2224–2227 (2014).
37. Leblanc, M., Maisonneuve, V. & Tressaud, A. Crystal chemistry and selected physical properties of inorganic fluorides and oxide-fluorides. *Chem. Rev.* **115**, 1191–1254 (2015).
38. Dzyaloshinsky, I. A thermodynamic theory of "weak" ferromagnetism of antiferromagnetics. *J. Phys. Chem. Solids* **4**, 241–255 (1958).
39. Moriya, T. Anisotropic superexchange interaction and weak ferromagnetism. *Phys. Rev.* **120**, 91–98 (1960).
40. Hohenberg, P. & Kohn, W. Inhomogeneous electron gas. *Phys. Rev.* **136**, B864 –B871 (1964).
41. Blöchl, P. E. Projector augmented-wave method. *Phys. Rev. B* **50**, 17953–17979 (1994).
42. Kresse, G. & Hafner, J. Ab initio molecular dynamics for liquid metals. *Phys. Rev. B.* **47**, 558–561 (1993).
43. Kresse, G. & Furthmüller, J. Efficiency of ab-initio total energy calculations for metals and semiconductors using a plane-wave basis set. *Comput. Mater. Sci.* **6**, 15–150 (1996).
44. Perdew, J. P., Burke, K. & Ernzerhof, E. Generalized gradient approximation made simple. *Phys. Rev. Lett.* **77**, 3865–3868 (1996).
45. Anisimov, V. I., Aryasetiawan, F. & Lichtenstein, A. I. First-principles calculations of the electronic structure and spectra of strongly correlated systems: the LDA + U method. *J. Phys: Condens. Matter.* **9**, 767–808 (1997).
46. King-Smith, R. D. & Vanderbilt, D. Theory of polarization of crystalline solids. *Phys. Rev. B.* **47**, R1651–R1654 (1993).
47. Resta, R. Macroscopic polarization in crystalline dielectrics: the geometric phase approach. *Rev. Mod. Phys.* **66**, 899–915 (1994).

Supplementary Information accompanies the paper on the *npj Quantum Materials* website (doi:10.1038/s41535-016-0001-8).